JACS
JOURNAL OF THE AMERICAN CHEMICAL SOCIETY

ARTICLE

pubs.acs.org/JACS

Pyochelin Enantiomers and Their Outer-Membrane Siderophore Transporters in Fluorescent Pseudomonads: Structural Bases for Unique Enantiospecific Recognition

Karl Brillet,[†] Cornelia Reimmann,[‡] Gaëtan L. A. Mislin,[†] Sabrina Noël,[†] Didier Rognan,[§] Isabelle J. Schalk,*[,†] and David Cobessi*[,∥]

[†]UMR 7242 Biotechnologie et Signalisation Cellulaire, Université de Strasbourg-CNRS, Irebs—ESBS, Boulevard Sébastien Brant, 67412 Illkirch, France

[‡]Département de Microbiologie Fondamentale, Université de Lausanne, Bâtiment Biophore, Quartier UNIL-Sorge, CH-1015 Lausanne, Switzerland

[§]Laboratoire d'Innovation Thérapeutique, UMR 7200, Université de Strasbourg-CNRS, Faculté de Pharmacie 74, route du Rhin, 67401 Illkirch-Graffenstaden Cédex, France

[∥]Institut de Biologie Structurale J.-P. Ebel, Commissariat à l'Energie Atomique, Centre National de la Recherche Scientifique, Université Joseph Fourier, Groupe Synchrotron, 41 rue Jules Horowitz, 38027 Grenoble, France

Supporting Information

ABSTRACT: Pyochelin (Pch) and enantiopyochelin (EPch) are enantiomeric siderophores, with three chiral centers, produced under iron limitation conditions by *Pseudomonas aeruginosa* and *Pseudomonas fluorescens*, respectively. After iron chelation in the extracellular medium, Pch—Fe and EPch—Fe are recognized and transported by their specific outer-membrane transporters: FptA in *P. aeruginosa* and FetA in *P. fluorescens*. Structural analysis of FetA—EPch—Fe and FptA—Pch—Fe, combined with mutagenesis and docking studies revealed the structural basis of the stereospecific recognition of these enantiomers by their respective transporters. Whereas FetA and FptA have a low sequence identity but high structural homology, the Pch and EPch binding pockets do not share any structural homology, but display similar physicochemical properties. The stereospecific recognition of both enantiomers by their corresponding transporters is imposed by the configuration of the siderophore's C4″ and C2″ chiral centers. This recognition involves specific hydrogen bonds between the Arg91 guanidinium group and EPch—Fe for FetA and between the Leu117—Leu116 main chain and Pch—Fe for FptA. FetA and FptA are the first membrane receptors to be structurally described with opposite binding enantioselectivities for their ligands, giving insights into the structural basis of their enantiospecificity.

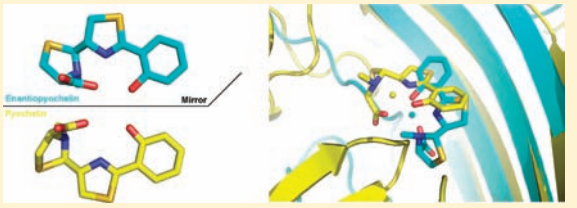

INTRODUCTION

Under conditions of iron limitation, pseudomonads produce and secrete iron-chelating compounds called siderophores into their environment.[1] These compounds bind ferric iron with high affinity and transport it back into the bacterial cells, via specific TonB-dependent transporters (TBDTs).[2] This uptake process is an energy-consuming mechanism involving interactions between a small periplasmic region of the TBDT called the TonB-box and the TonB—ExbB—ExbD complex located in the inner membrane.[3]

Pyochelin (Pch) is a siderophore isolated from iron-deficient cultures of *Pseudomonas aeruginosa* ATCC 15692 (strain PAO1), and its structure was established as 2′-(2-hydroxyphenyl)-3″-methyl-4″,5′,2″,3″,4″,5″-hexahydro-[4′,2″]bithiazolyl-4″-carboxylic acid.[4,5] Pch presents three chiral centers at the C4′, C2″, and C4″ positions and is extracted as a mixture of two interconvertible diastereoisomers whose absolute configuration are 4′*R*,2″*R*,4″*R* (Pch I) and 4′*R*,2″*S*,4″*R* (Pch II).[6] Iron(III) and zinc(II) were shown to induce a shift from Pch II to Pch I by converting the *S* configuration of the C2″ chiral center into the *R* configuration.[7,8] Pch chelates Fe^{3+} with a 2:1 (Pch/Fe(III)) stoichiometry,[6,9] with one molecule of Pch tetradentately coordinated to Fe^{3+} and the second molecule bound bidentately to complete the hexacoordinate octahedral geometry.[9] Enantiopyochelin (EPch), the enantiomer of Pch, was isolated from *Pseudomonas fluorescens* as a mixture of the two diastereoisomers with absolute configurations established as 4′*S*,2″*S*,4″*S* (EPch I) and 4′*S*,2″*R*,4″*S* (EPch II) (Figure 1).[10] It is likely that the metal-induced epimerization of the C2″ chiral center, observed for the natural Pch diastereoisomers pair, exists also for the two EPch diastereoisomers. For the sake of clarity, in the present article, the terms Pch and EPch thus refer, respectively, to the enantiomers Pch I and EPch I who are predominant in the presence of iron(III).

Received: June 14, 2011
Published: September 08, 2011

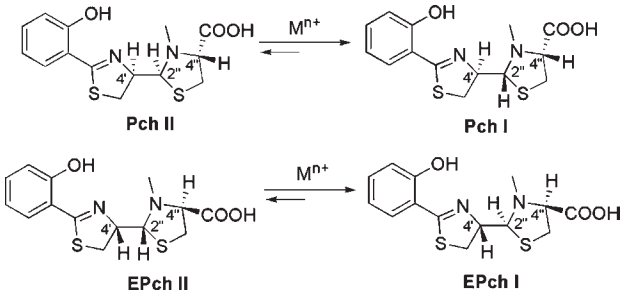

Figure 1. Structures, and absolute configurations, of naturally occurring diastereoisomers of pyochelin (Pch I/Pch II) and enantiopyochelin (EPch I/EPch II) siderophores of, respectively, *P. aeruginosa* and *P. fluorescens*. The metal-induced epimerization (M^{n+}) on the C2″ position has only been shown for Pch.

Pch−Fe and EPch−Fe are specifically recognized and transported by the outer-membrane transporters FptA expressed by *P. aeruginosa* and FetA expressed by *P. fluorescens*.[11] Binding and iron uptake assays showed that FptA recognized (K_d = 2.5 ± 1.1 nM) and transported Pch−Fe but failed to do so with EPch−Fe. Correspondingly, FetA was specific for EPch−Fe (K_d = 3.7 ± 2.1 nM) but did not interact with Pch−Fe. Growth promotion experiments performed under conditions of iron limitation confirmed that FptA and FetA were highly specific for Pch and EPch, respectively, and were able to discriminate the two enantiomers.[12]

The crystal structure of FptA loaded with Pch−Fe (Figure 2A) was solved at 2 Å resolution.[13] FptA, as all TBDTs, can be divided into two domains: a 22 β-stranded transmembrane barrel which is occluded by the N-terminal domain, also called the plug domain. The Pch−Fe binding pocket is on the extracellular face and is mainly composed of hydrophobic and aromatic residues from the plug and the barrel, consistent with the hydrophobicity of Pch. In the crystal structure, Pch provided a tetradendate coordination of iron and the remaining bidentate coordination was provided by ethylene glycol used in the crystallization condition. This suggested that only one Pch molecule is necessary for recognition by FptA.[13] In addition, binding assays and docking experiments using synthetic Pch analogues showed that the specific recognition of Pch−Fe by FptA was probably due to the configuration of the C4″ and C2″ chiral centers, and was weakly dependent on the configuration of the C4′ carbon atom.[14]

In the present study, we solved the three-dimensional (3D) structure of FetA bound to EPch−Fe at 3.2 Å resolution. The structural comparison of FetA and FptA binding pockets combined with molecular biology and docking experiments identified the molecular basis of the enantiospecific recognition in the Pch/FptA and EPch/FetA ligand/receptor pairs. Although stereospecific recognition between chiral siderophores and their outer-membrane receptor has already been described,[15−22] the enantiospecific discrimination of Pch and EPch by the FptA and FetA receptors is unique in bacterial iron uptake systems.

RESULTS

Construction and in Vivo Activity of Histidine-Tagged FetA. Using our cloning-to-crystallization protocol for TBDTs,[23] we constructed a FetA derivative with a histidine tag in extracellular loop 5 to facilitate subsequent protein purification by

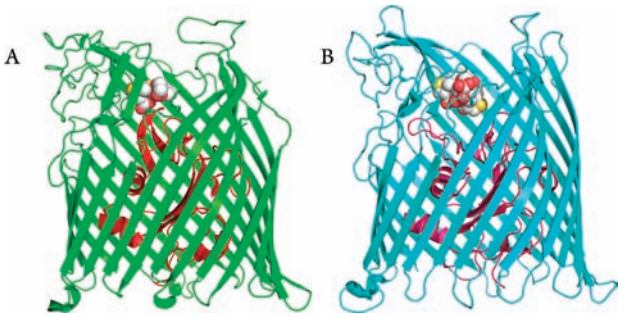

Figure 2. (A) FptA overall structure.[13] The plug and the β-barrel are shown in red and green color. Pch−Fe−ethylene glycol is displayed in van der Waals spheres. (B) FetA overall structure. The plug and the β-barrel are shown in purple and cyan color. EPch−Fe−citrate is displayed in van der Waals spheres.

affinity. To verify the biological activity of histidine-tagged FetA, we tested whether pME7583, which expresses the tagged *fetA* gene regulated by the *tac* promoter, would be able to complement a *fetA* mutation in *P. fluorescens* for growth promotion by EPch. Supporting Information Figure S1 shows that unmodified M9−glycerol medium contained sufficient iron to support growth of the siderophore-negative *P. fluorescens* strain CHA1085 and its *fetA*-deletion derivative CHA1169. However, no strain could grow when the iron chelator 2,2′-dipyridyl was added to the medium. Addition of EPch restored growth in CHA1085 and in the strain expressing the His-tagged FetA (CHA1169 carrying pME7583), whereas the siderophore did not promote growth in the plasmid-free CHA1169 strain. FetA is thus essential for EPch-mediated iron uptake in *P. fluorescens* as reported previously,[10,12] and the histidine-tagged FetA protein is active in vivo.

FetA Overall Structure. The asymmetric unit contained two monomers of FetA. Apart from the Ser577−Lys585 loop, they superimposed with a 0.56 Å rmsd value and interacted by the membrane part. FetA is folded into two domains: a C-terminal 22-stranded β-barrel (residues Lys160−Trp698) whose lumen is occluded by an N-terminal plug domain (residues Pro23−Asp159) (Figure 2B). The plug domain is composed by a mixed four-stranded β-sheet and contained two α-helices. It is stabilized into the lumen of the β-barrel by numerous hydrogen bonds and van der Waals contacts. The β-strands of the transmembrane β-barrel are connected by periplasmic turns and long extracellular loops that probably participate to binding and transport of the ligand. The first 22 residues containing the TonB-box and histidines originating from the tag inserted into extracellular loop L5 were not observed in the electron density. One sulfate ion was bound to FetA and stabilized by Arg330, Arg332, and Tyr371. The rmsd values calculated using SSM[24] range from 1.40 Å (FetA/FhuA, PDB entry 1BY5[25]) up to 2.67 Å (FetA/FepA, PDB entry 1FEP[26]), from comparison with the other TBDTs of known structure.

EPch−Fe Binding Pocket in FetA. A large peak of positive electron density corresponding to the ligand was observed at the FetA extracellular face. Iron was first placed, and using the phases calculated from FetA−Fe, two sulfur atoms were added into the Fo−Fc electron density map after contouring the map beyond 9σ. EPch−Fe was positioned into the electron density based on the sulfur atoms and iron positions, resulting in positive electron density corresponding to a second chelating molecule

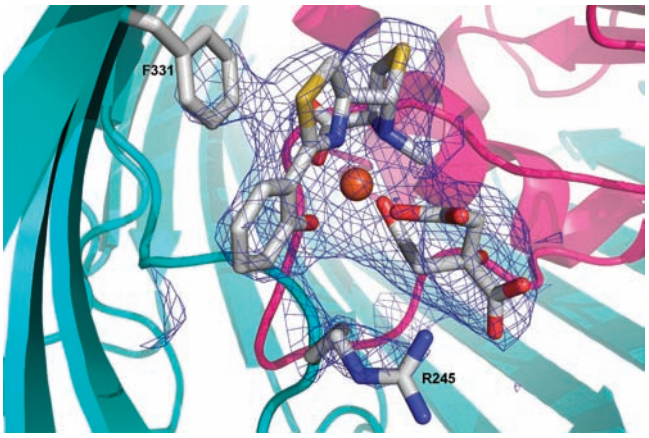

Figure 3. Resulting electron density map of the ligand binding site. FetA is shown as a ribbon. EPch−Fe−citrate is superposed onto the 2FoFc electron density map contoured at 1.2σ.

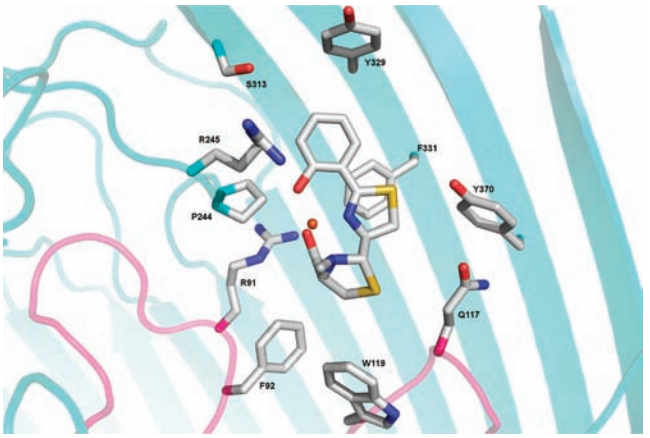

Figure 4. View of the EPch−Fe binding pocket of FetA. EPch−Fe, Arg91, Phe92, Gln117, Trp119, Pro244, Arg245, Ser313, Tyr329, Phe331, and Tyr370 are displayed as sticks. The hydrogen bond between Arg91 and EPch is represented by a dashed line. For clarity, citrate was removed.

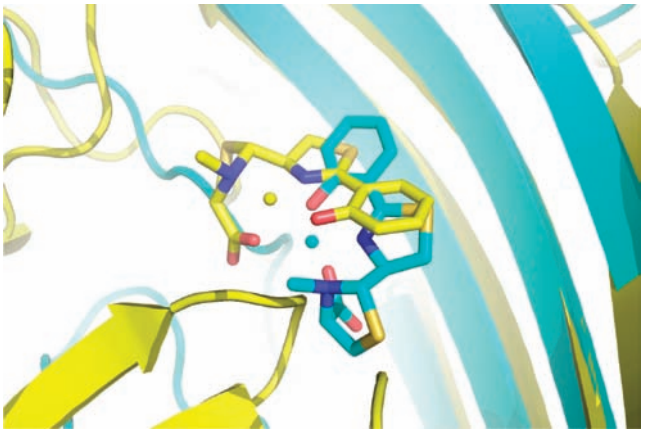

Figure 5. Superimposition of FetA−EPch−Fe and FptA−Pch−Fe showing the location of the ligands. FptA and FetA are colored yellow and cyan, respectively. The Pch and EPch carbon atoms are colored yellow and cyan, respectively.

(Supporting Information Figure S2). However, this density could not be attributed to another EPch molecule. Citrate, an iron chelating agent, used in the crystallization conditions was added to the model (Figure 3). After refinement, the B-factors average for citrate was higher than that for EPch−Fe (79.90 vs 65.97 Å^2; B-factor average EPch−Fe−citrate, 71.15 Å^2). This suggests disorder resulting from its solvent exposure and the absence of interaction with FetA, apart from Arg245 (B-factor average, 78.24 Å^2; B-factor overall, 70.50 Å^2) also exposed to solvent. The electron density of Arg245 was different between both molecules in the asymmetric unit suggesting flexibility.

The binding pocket is located at the extracellular face and is composed mainly of hydrophobic residues from the plug and barrel domain. EPch−Fe is stabilized by several van der Waals interactions (distances less than 4 Å calculated with PDBeMotif[27]) with Phe92, Gln117, Trp119, Pro244, Arg245, Ser313, Tyr329, Phe331, and Tyr370 whose hydroxyl group is 3.2 Å apart from the sulfur atom of the thiazolin ring (Figure 4 and Supporting Information Table S1).

A hydrogen bond is also observed between the carboxylate group of thiazolidin ring and the Arg91 side chain (Figure 4). Although the Tyr370 hydroxyl group is 3.2 Å apart from the sulfur atom of the thiazolin ring of EPchFe, both entities appear to be not well-oriented to be involved in a hydrogen bond. Arg91 and Tyr370 were mutated to Ala to evaluate their importance in the binding of EPch−Fe. In the case of FetA$_{R91A}$, this mutation resulted in a loss of binding of EPch−^{55}Fe, indicating that Arg91 has a key role in the positioning of the ferrisiderophore into the binding pocket. However, with FetA$_{Y370A}$, this mutation resulted in only a 3-fold increase in dissociation constant (K_d = 2.4 ± 0.4 nM for FetA and K_d = 7.5 ± 0.7 nM for FetA$_{Y370A}$), suggesting a less important role for Tyr370. Therefore, there is no other hydrogen bond than that between Arg91/EPch−Fe which may contribute strongly to the overall binding affinity. The other stabilizing contacts are van der Waals interactions between EPch−Fe and several residues of the binding site like Tyr370 (Supporting Information Table S1). The topology of the binding pocket was compared with the structures from PDB using RASMOT3D[28] and PDBeMotif[27] at EBI, and no identical binding site was found in any of the proteins of known structure.

Comparison of FetA with FptA. The structure-based sequence alignment between FetA and FptA showed a sequence identity of 25.1% (Supporting Information Figure S3A). FptA (Figure 2A) and FetA (Figure 2B) superimposed with an rmsd value of 1.77 Å (Supporting Information Figure S3, parts B and C), and their PchFe and EPchFe ligands partly overlapped (Figure 5). In both structures, the binding pocket is hydrophobic and delineated by residues from the plug and β-barrel domains, but none of these residues are conserved (Supporting Information Figure S3, parts A and D). Pch−Fe bound to FptA is stabilized by Phe114, Leu116, and Leu117, which belong to an apical loop of the plug domain. In FetA, Arg91 from the first apical loop and Gln117 as well as Trp119 from the second apical loop are part of the binding pocket (Figure 4). Phe331 of FetA superimposes onto Tyr356 of FptA, and Tyr370 located in the β-strand β9 of FetA superimposed onto Glu395 of FptA, which is involved in the stabilization of PchFe. In both cases, only one Pch−Fe or EPch−Fe molecule is inside the binding pocket and the second iron-chelating molecule originating from the crystallization solutions is always exposed toward the solvent. Ethylene glycol and citrate are bound to Fe instead of Pch and EPch

Table 1. Docking Statistics of Pch−Fe and EPch−Fe to the X-ray Structures of FptA and FetA

	outer-membrane transporter					
	FptA			FetA		
ligand	GOLD score[a]	Tc−IFP[b]	rmsd, Å[c]	GOLD score	Tc−IFP[d]	rmsd, Å[e]
Pch−Fe	53.16	0.81	0.40	46.96	0.55	
EPch−Fe	52.11	0.72		58.96	0.87	1.59

[a] Docking score using standard GOLD v5.0[58] docking settings. [b] Similarity of the protein−ligand interaction fingerprint (expressed by the Tc Tanimoto coefficient) to that of the FptA−Pch−Fe X-ray structure, as measured by the IFP[60] program. [c] Root-mean-square deviation (heavy atoms) to the X-ray pose of FptA-bound Pch−Fe. [d] Similarity of the protein−ligand interaction fingerprint (expressed by the Tc Tanimoto coefficient) to that of the FetA−EPch−Fe X-ray structure, as measured by the IFP program. [e] Root-mean-square deviation (heavy atoms) to the X-ray pose of FetA-bound EPch−Fe.

because they are in crystallization solutions at concentrations higher than those of EPch or Pch. Since they are also metal chelators, they compete with Pch and EPch for iron binding. Superimposition of EPch−Fe−citrate and Pch−Fe−ethylene glycol showed that citrate and ethylene glycol are in opposite positions to each other, which is due to the configuration of the C2″ and C4″ chiral centers in Pch and EPch (Supporting Information Figure S4). Despite the different amino acid contents of the siderophore binding sites in FetA and FptA, and the different ways of binding the corresponding ferrisiderophore, the 3D physicochemical properties like volume, buriedness, curvature, and balance between hydrophilic and hydrophobic properties of both binding pockets are very similar according to SiteAlign[29] (d1 score = 0.58; d2 score = 0.17) and FuzCav[30] (similarity = 0.218). This is probably related to the common form and hydrophobicity of the two ligands.

Ligand Docking. Pch−Fe and EPch−Fe could be redocked into the X-ray structures of FptA and FetA with low rms deviations to protein-bound ligand X-ray coordinates and high interaction fingerprint similarity (Table 1). Cross-docking of Pch−Fe in FetA (Figure 6A) and of EPch−Fe in FptA (Figure 6B) led to slightly lower docking scores and much lower interaction fingerprint similarities. In both cases, crucial hydrogen bonds to Leu116 and Leu117 main chain nitrogen atoms (in FptA) or Arg91 side chain (in FetA) could not be found when docking the wrong enantiomer.

DISCUSSION

Although the origin of chirality in biomolecules remains unclear, this structural property is essential to the chemistry of life.[31] Stereospecific interactions between ligands and receptors are involved in many crucial biological processes. Understanding the structural basis of interactions between proteins and chiral ligands is therefore not only a fascinating topic in the field of protein chemistry but also has tremendous implications in pharmacology and drug design.[32]

In this context, we investigated the stereospecific interaction of an enantiomeric ligand pair (Pch and EPch) with their cognate receptors (FptA and FetA). Although FptA and FetA share only 25.1% identical amino acids (Supporting Information Figure S3A), both transporters adopt the classical fold of TBDTs

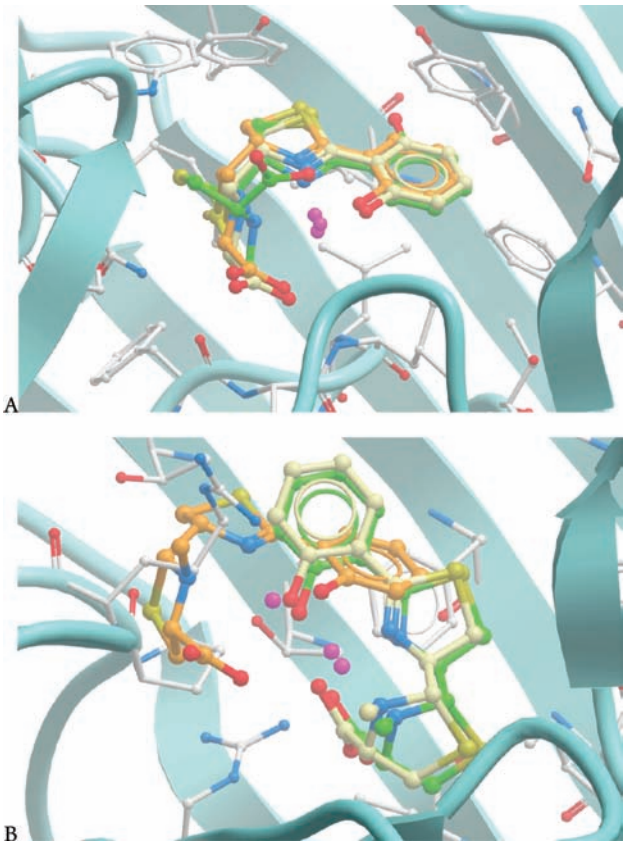

Figure 6. Docking of Pch−Fe and EPch−Fe on FetA (A) and FptA (B) binding sites, respectively. (A) Predicted binding mode of Pch−Fe (orange carbon atoms) and EPch−Fe (green carbon atoms) to the X-ray structure of FptA (cyan ribbons). The X-ray pose of FptA-bound Pch−Fe (yellow carbon atoms) is shown for comparison. FptA residues lining the Pch binding site are displayed as white carbon atoms. Iron atoms are indicated by magenta balls. Nitrogen, oxygen, and sulfur atoms are colored in blue, red, and yellow, respectively. (B) Predicted binding mode of Pch−Fe (orange carbon atoms) and EPch−Fe (green carbon atoms) to the X-ray structure of FetA (cyan ribbons). The X-ray pose of FetA-bound EPch−Fe (yellow carbon atoms) is shown for comparison. FetA residues lining the EPch binding site are displayed as white carbon atoms. Iron atoms are indicated by magenta balls. Nitrogen, oxygen, and sulfur atoms are colored in blue, red, and yellow, respectively.

(Figure 2). In both cases, only one siderophore molecule was observed in the electron density map at the extracellular face of the receptor. EPch and Pch thus provide the tetradendate coordination to iron and the remaining two coordination bonds are ensured by another ligand. In the crystal structures of FptA[13] and FetA (the present study), this ligand originated from the crystallization conditions as the binding pockets of both receptors occupied by their cognate ferrisiderophore are accessible to the solvent. In vivo, this ligand may be a second siderophore or another chelator present in the environment. Indeed, we previously showed that a mixed complex of Pch, iron, and cepabactin[33] (a siderophore produced by *Burkholderia cepacia*) can bind to FptA.[14] Therefore, only one Pch or EPch molecule is likely to be necessary for recognition by FptA or FetA, respectively.

The main differences between FetA and FptA are the amino acid composition of the ferrisiderophore binding pocket and their interactions with Pch−Fe or EPch−Fe. Despite these

differences, both binding sites were seen to partly overlap, when FetA was superimposed onto FptA, and they have similar 3D physicochemical properties and a common form. Due to the opposite configuration of the two chiral centers C2″ and C4″, EPch−Fe and Pch−Fe are observed in different orientations within the binding pockets (Figure 4). However, in both cases, the carboxylate group of the siderophores interacted via hydrogen bonds with residues of the plug domain: the Arg91 guanidinium group in FetA and the Leu116 and Leu117 nitrogen in FptA.[13] Mutagenesis experiments and docking assays confirmed that these hydrogen bonds are essential for the specific interactions between the two siderophores and their receptor. Despite the similar physicochemical properties of the binding pocket, two different interaction networks therefore allow FetA and FptA to discriminate the enantiomeric ferrisiderophores where configuration of the C2″ and C4″ chiral centers is crucial for receptor specificity. Indeed, the C4″ chiral center bears the carboxylate group involved in the hydrogen bond for the siderophore binding to its specific receptor, and a cis geometry for the two hydrogen atoms on the C4″ and C2″ position is necessary for an optimal iron(III) chelation.

During the course of evolution, two transporters have probably been selected with low sequence identity but a similar structure to specifically recognize enantiomers through different interactions in similar binding pockets. Enantiospecificity is also observed in other proteins involved in the regulation of the Pch/EPch-dependent iron uptake systems.[34] EPch−Fe and Pch−Fe induce the expression of their biosynthesis genes through interactions with PchR, an AraC-type transcriptional regulator. Recent studies showed that the recognition of EPch and Pch by their respective PchR regulator is highly enantiospecific.[34]

Stereospecificity of siderophore-dependent iron uptake has been previously reported for parabactin, rhodotorulic acid, rhizoferrin, ferrichrome, and enterobactin.[15−22] In this context, the polycarboxylate siderophore, rhizoferrin, is of particular interest as it naturally exists as two biologically relevant enantiomers. (*S*,*S*)-rhizoferrin is synthesized by several strains of *Ralstonia* (formerly *Pseudomonas*) *picketii*, whereas (*R*,*R*)-rhizoferrin is produced by *Zygomycetes* fungi. In *Ralstonia*, rhizoferrin-dependent iron uptake transports both iron-loaded enantiomers with the same efficiency. In contrast, rhizoferrin-mediated iron uptake appears to be partially enantioselective in the fungus *Rhizopus* where iron uptake with (*R*,*R*)-rhizoferrin is twice as efficient as with (*S*,*S*)-rhizoferrin.[22] A similar comparative study on ferrichrome-dependent iron uptake in *Escherichia coli* and certain fungi (*Neurospora*, *Penicillium*) showed that fungi preferably used only one siderophore enantiomer, whereas the bacterium could use both optical antipodes of ferrichrome.[20] Prokaryotic siderophore-dependent iron uptake systems therefore appear poorly stereo- or enantiospecific, whereas the corresponding eukaryotic iron transport pathways have a higher stereospecificity.[21]

To date, no crystallographic data of these bacterial and fungal receptors are available which could help to understand the structural basis of the differences in specificity. A survey of prokaryotic and eukaryotic protein−ligand complexes in the Protein Data Bank did not reveal a single pair of enantiomeric ligands cocrystallized with two different membrane receptors. Although there are drugs (e.g., butaclamol) with inverted eudismic ratio (ratio of the affinity values of both stereisomers) to different G protein-coupled receptors,[35] their binding sites are very similar.[36] Likewise, some terpenes (e.g., limonene, carvone) exhibit stereospecific odors by binding to different olfactory receptors.[37] However, no structural data are available to describe the structural basis of stereospecificity in these systems. Thus, FetA from *P. fluorescens* and FptA from *P. aeruginosa* are, to our knowledge, unique examples of two membrane transporters structurally characterized with a strictly opposite binding enantioselectivity due to nonidentical binding pockets.

EXPERIMENTAL METHODS

Construction of Plasmids and Gene Replacement Mutants. DNA cloning and plasmid preparations were carried out according to standard procedures.[38] Strains, plasmids, and oligonucleotides used in this work are listed in Supporting Information Table S2. Constructs generated by polymerase chain reaction (PCR) were verified by sequence analysis with the BigDye Terminator Cycle Sequencing kit and an ABI-PRISM 373 automatic sequencer from Applied Biosystems. A modified *fetA* gene specifying a receptor protein with an internal histidine tag was constructed by overlap extension PCR and cloned under the IPTG-inducible *tac* promoter of plasmid pME6032 as follows. Two PCR fragments of 0.95 kb and 1.35 kb carrying the 3′ and 5′ parts of *fetA*, respectively, were generated from chromosomal DNA of *P. fluorescens* CHA0 using the primer pairs fetAhis-1/fetAhis-2 and fetAhis-3/fetAhis-4. The two PCR fragments were then combined by a second PCR cycle using the primers fetAhis-2 together with fetAhis-3. This generated a 2.3 kb fragment which was subsequently cleaved with *Eco*RI and *Bgl*II and cloned into the same sites on pME6032 giving pME7583. The insert was verified by sequence analysis which confirmed the presence of five additional histidine residues downstream of the already existing histidine at position 387. Gene replacement mutants of *P. fluorescens* were obtained with suicide plasmids as described previously.[39,40] The suicide plasmid pME9605, used to generate a 882 bp in-frame deletion in the pyoverdine biosynthesis gene *pvdF*, was constructed as follows. Two PCR fragments were generated from chromosomal DNA of *P. fluorescens* CHA0 using the primer pairs PFL4090-1/PFL4090-2 and PFL4090-3/PFL4090-4. The two fragments were then joined by overlap extension PCR using PFL4090-1 and PFL4090-4. This generated a 1.5 kb fragment which was trimmed with *Bam*HI and *Eco*RI and subsequently cloned into the suicide vector pME3087 giving pME9605. This construct was then mobilized from *E. coli* DH5α to *P. fluorescens* CHA1084 (Δ*pchDHIEFKCBA*) using the helper plasmid pME497 and chromosomally integrated, with selection for Tc (100 μg mL^{-1}) and Cm (10 μg mL^{-1}). Plasmid excision via a second crossing-over was obtained through enrichment for Tc-sensitive cells as described.[39,40] Among these, mutants with deletions in *pvdF* were identified by PCR and named CHA1239 (Δ*pchDHIEFKCBA* Δ*pvdF*). The two CHA1239 derivatives CHA1343 (Δ*pvdF* Δ*pchDHIEFKCBA* $fetA_{R91A}$) and CHA1344 (Δ*pvdF* Δ*pchDHIEFKCBA* $fetA_{Y370A}$) with single amino acid changes in *fetA* were obtained in a similar way using the suicide plasmids pME9644 and pME9645, respectively. Construction of pME9644 was done with the primer pairs R91-1/R91-2 and R91-3/R91-4. Fragment joining by overlap extension PCR involved the primer pair R91-1/R91-4 and cloning into pME3087 was done with *Bam*HI and *Hin*dIII. Overlap extension PCR was also used to generate pME9645, the primers involved were Y370-1, Y370-2, Y370-3, and Y370-4. Again, cloning into pME3087 was done with *Bam*HI and *Hin*dIII. Mutants were generated by gene replacement as described above and identified by sequencing the chromosomal *fetA* gene amplified by PCR.

Culture Conditions. Bacteria were routinely grown on nutrient agar and in nutrient yeast broth or LB[38,41] at 37 °C (*E. coli*) or 30 °C (*P. fluorescens*). Siderophore-mediated growth promotion assays were carried out in minimal medium M9[38] with 0.5% glycerol as a carbon source as described.[12] Iron limitation was achieved in this medium with 500 μM 2,2′-dipyridyl. For expression and purification

of histidine-tagged FetA, bacteria were grown in LB medium amended with 1 mM isopropyl β-D-1-thiogalactopyranoside (IPTG). Where necessary, tetracycline (Tc) was added to the growth media at 25 μg/mL for *E. coli* and 100 μg/mL for *P. fluorescens*. To counterselect *E. coli* donors in gene replacement experiments, chloramphenicol (Cm) was added at 10 μg/mL. Mutant enrichment occurred with Tc at 20 μg/mL and cycloserine at 50 mg/mL.

Ligand-Binding Assays Using ^{55}Fe (Supporting Information Figure S5). EPch−^{55}Fe was prepared as described previously.[12] To determine the apparent dissociation constants in vivo of EPch−^{55}Fe binding to FetA and FetA mutants, CHA1085, CHA1343, and CHA1344 cells were washed twice with an equal volume of fresh medium and resuspended in 50 mM Tris−HCl (pH 8.0) buffer at an OD_{600nm} of 1.5. The cells were then incubated at 0 °C to avoid any iron uptake for 1 h in a final volume of 500 μL in the presence of various concentrations (0.1−600 nM) of siderophore−^{55}Fe. Incubations were stopped by centrifugation at 12 000 *g* (4 °C) for 2 min. The supernatant containing the unbound siderophore−^{55}Fe was removed, and the tubes containing the cell pellet were counted for radioactivity in a scintillation cocktail.[42] The experiment was repeated with CHA1169 to estimate nonspecific interactions of EPch−^{55}Fe with the tubes or with the cells.

FetA Purification, Crystallization, and Data Collection. FetA was overexpressed in *P. fluorescens* and purified as described for FauA and ShuA.[23,43] The pure fractions containing FetA were pooled, dialyzed with 10 mM Tris−HCl pH 8.0 and 0.75% C8E5 (Bachem), and concentrated to 10 mg/mL. EPch was solubilized in methanol at a concentration of 74 mM, and $FeCl_3$ was added with a EPch/Fe ratio of 2:1. Prior to crystallization, EPch−Fe was added to FetA at a final concentration of 1.22 mM. Initial crystallization experiments were performed using the MbClass suite and MbClassII suite from QIAGEN, and improvements of the crystallization conditions were performed in LinbroPlates using the sitting-drop vapor-diffusion method at 293 K. FetA−EPch−Fe (10 mg/mL) was crystallized in 14% PEG1500, 0.1 M lithium sulfate, 0.1 M sodium citrate pH 5.6, 20% glycerol. The diffraction data were collected using synchrotron radiation at ESRF on BM30A[44] using an ADSC Q315r CCD detector (λ = 0.95024 Å). The data were collected using one crystal at 100 K, integrated and scaled at 3.25 Å resolution using XDS.[45] Crystals belong to the $C222_1$ space group (Table 2).

Structure Resolution. The phase problem was solved by molecular replacement using PHASER[46] from CCP4[47] and FhuA (PDB entry 1BY3[17]) as molecular model after replacing the nonconserved residues by alanine residues and after removing the nonaligned parts of sequences. The model was rebuilt at 3.25 Å resolution using COOT[48] and refined by energy minimization and molecular dynamic using Phenix[49] and by restrained maximum-likelihood least-squares techniques in REFMAC5[50] from CCP4.[47] During refinement of the FetA−EPch−Fe complex in which noncrystallographic symmetry was used, EPch−Fe and sulfate ions were added. Finally, citrate was added into a large peak of positive electron density close to the ferric iron. At the end of the refinement the *R* and Rfree[51] factors were 21.4% and 25.9%, respectively (Table 2). The model was checked using PROCHEK,[52] WHATCHECK,[53] and MOLPROBITY.[54] All the drawing were prepared using Pymol.[55]

Ligand Docking. The starting conformation of Pch−Fe and EPch−Fe were obtained by converting SymyxDraw[56] two-dimensional (2D) sketches into 3D coordinates using the Corina 3.10 program.[57] Automated docking of manually ionized ligands to the FptA X-ray structure (PDB code 1XKW) and the herein described FetA structure was done using standard settings of the GOLD v5.0 program.[58] All organic molecules were first removed from the protein structure, and hydrogen atoms automatically added using the Biopolymer module of the SYBYL-X1.2 package.[59] The active site used for sampling the conformational space of the ligand was defined by a 10 Å radius sphere centered on the center of mass of Pch−Fe (FptA) and EPch−Fe (FetA). To further speed up the calculation, docking was stopped when the top three ranked solutions were within 1.5 Å rmsd. If this criterion is met, we can assume that these top solutions represent a reproducible pose for the ligand. A maximum of 30 poses were saved for each ligand in standard mol2 format and ranked by decreasing GOLDscore. For each pose, an interaction fingerprint was computed using the IFP program[60] and compared to that of the FptA−Pch and FetA−EPch X-ray structures, respectively, using a standard Tanimoto coefficient.

Table 2.[a]

Diffraction Data	
resolution (Å)	48.57−3.26 (3.34−3.26)
wavelength (Å)	0.95024
unit cell (Å)	a = 155.07 b = 170.83 c = 232.62
space group	$C222_1$
no. of unique reflections	48366 (3436)
completeness (%)	99.3 (96.4)
redundancy	8.2 (8.1)
Rsym (%)[b]	13.7 (65.9)
$I/\sigma(I)$	16.11 (3.57)
structure refinement	48.57−3.26 (3.26−3.34)
Rcryst (%)[c]	21.4 (29.6)
Rfree (%)	25.9 (39.6)
$F/\sigma F$	0
no. of protein atoms	10449
no. of ligand atoms	80
rms deviation of bond lengths (Å)	0.017
rms deviation of bond angles (deg)	2.079
av B factor (Å^2)	70.49

[a] Numbers between parentheses indicate the value in the outer resolution shell. The Rfree was calculated using 5% reflections, which were kept apart from the refinement during the whole process. rms = root-mean-square. [b] Rsym = ΣΣ|Ii − Im|/ΣΣIi, where Ii is the intensity of the measured reflection and Im is the mean intensity of this reflection. [c] Rcryst = Σ||Fobs| − |Fcalc||/Σ|Fobs|. Rfree is the same as Rcryst but calculated for 5% data omitted from the refinement.

■ ASSOCIATED CONTENT

Supporting Information. One table giving distances between EPchFe and FetA; one table describing all bacterial strains, plasmids, and oligonucleotides used in this study; growth curves showing that the His-tagged FetA receptor is active in iron uptake; a sequence alignment deduced from the superposition of FetA/FptA; two views of superimposition of FetA onto FptA, a superimposition of binding pockets from FetA and FptA from the superimposition of FetA onto FptA, a superimposition of EPch−Fe−citrate and Pch−Fe−ethylene glycol from FetA−EPch−Fe−citrate and FptA−Pch−Fe−ethylene glycol, and a Scatchard analysis of the binding of EPch−^{55}Fe to FetA in vivo. This material is available free of charge via the Internet at http://pubs.acs.org.

■ AUTHOR INFORMATION

Corresponding Author
isabelle.schalk@unistra.fr; david.cobessi@ibs.fr

■ ACKNOWLEDGMENT

We thank Jeremy Perrin for his help with mutant construction. This work was supported by the Centre National de la Recherche Scientifique (CNRS), the association Vaincre la Mucoviscidose (French Association against cystic fibrosis), the Agence Nationale de Recherche (Grant ANR-08-BLAN-0315-01), and the Swiss National Science Foundation for Scientific Research (project 31003A_132998).

■ REFERENCES

(1) Hider, R. C.; Kong, X. L. *Nat. Prod. Rep.* **2010**, *27*, 637–657.
(2) Noinaj, N.; Guillier, M.; Barnard, T. J.; Buchanan, S. K. *Annu. Rev. Microbiol.* **2010**, *64*, 43–60.
(3) Postle, K.; Larsen, R. A. *Biometals* **2007**, *20*, 453–465.
(4) Cox, C. D. *J. Bacteriol.* **1980**, *142*, 581–587.
(5) Cox, C. D.; Rinehart, K. L., Jr.; Moore, M. L.; Cook, J. C., Jr. *Proc. Natl. Acad. Sci. U.S.A.* **1981**, *78*, 4256–4260.
(6) Ankenbauer, R. G.; Toyokuni, T.; Staley, A.; Rinehart, K. L., Jr.; Cox, C. D. *J. Bacteriol.* **1988**, *170*, 5344–5351.
(7) Rinehart, K. L.; Staley, A. L.; Wilson, S. R.; Ankenbauer, R. G.; Cox, C. D. *J. Org. Chem.* **1995**, *60*, 2786–2791.
(8) Ino, A.; Murabayashi, A. *Tetrahedron* **2001**, *57*, 1897–1902.
(9) Tseng, C. F.; Burger, A.; Mislin, G. L. A.; Schalk, I. J.; Yu, S. S.-F.; Chan, S. I.; Abdallah, M. A. *J. Biol. Inorg. Chem.* **2006**, *11*, 419–432.
(10) Youard, Z. A.; Mislin, G. L. A.; Majcherczyk, P. A.; Schalk, I. J.; Reimmann, C. *J. Biol. Chem.* **2007**, *282*, 35546–35553.
(11) Youard, Z. A.; Wenner, N.; Reimmann, C. *Biometals* **2011**, *24*, 513–522.
(12) Hoegy, F.; Lee, X.; Noël, S.; Mislin, G. L. A.; Rognan, D.; Reimmann, C.; Schalk, I. J. *J. Biol. Chem.* **2009**, *284*, 14949–14957.
(13) Cobessi, D.; Celia, H.; Pattus, F. *J. Mol. Biol.* **2005**, *352*, 893–904.
(14) Mislin, G. L. A.; Hoegy, F.; Cobessi, D.; Poole, K.; Rognan, D.; Schalk, I. J. *J. Mol. Biol.* **2006**, *357*, 1437–1448.
(15) Bergeron, R. J.; Dionis, J. B.; Elliott, G. T.; Kline, S. J. *J. Biol. Chem.* **1985**, *260*, 7936–7944.
(16) Bergeron, R. J.; Xin, M. G.; Weimar, W. R.; Smith, R. E.; Wiegand, J. *J. Med. Chem.* **2001**, *44*, 2469–2478.
(17) Drechsel, H.; Jung, G.; Winkelmann, G. *Biometals* **1992**, *5*, 141–148.
(18) Muller, G.; Isowa, Y.; Raymond, K. N. *J. Biol. Chem.* **1985**, *260*, 13921–13926.
(19) Neilands, J. B.; Erickson, T. J.; Rastetter, W. H. *J. Biol. Chem.* **1981**, *256*, 3831–3832.
(20) Winkelmann, G. *FEBS Lett.* **1979**, *97*, 43–46.
(21) Winkelmann, G.; Braun, V. *FEMS Microbiol. Lett.* **1981**, *11*, 237–241.
(22) Münzinger, M.; Taraz, K.; Budzikiewicz, H.; Drechsel, H.; Heymann, M.; Winkelmann, G.; Meyer, J.-M. *Biometals* **1999**, *12*, 189–193.
(23) Brillet, K.; Meksem, A.; Lauber, E.; Reimmann, C.; Cobessi, D. *Acta Crystallogr., Sect. D* **2009**, *65*, 326–331.
(24) Krissinel, E.; Henrick, K. *Acta Crystallogr., Sect. D* **2004**, *60*, 2256–2268.
(25) Locher, K. P.; Rees, B.; Koebnik, R.; Mitschler, A.; Moulinier, L.; Rosenbusch, J. P.; Moras, D. *Cell* **1998**, *95*, 771–778.
(26) Buchanan, S. K.; Smith, B. S.; Venkatramani, L.; Xia, D.; Esser, L.; Palnitkar, M.; Chakraborty, R.; van der Helm, D.; Deisenhofer, J. *Nat. Struct. Biol.* **1999**, *6*, 56–63.
(27) Golovin, A.; Henrick, K. *BMC Bioinf.* **2008**, *9*, 312.
(28) Magis, C.; Gasparini, D.; Lecoq, A.; Le Du, M. H.; Stura, E.; Charbonnier, J. B.; Mourier, G.; Boulain, J. C.; Pardo, L.; Caruana, A.; Joly, A.; Lefranc, M.; Masella, M.; Menez, A.; Cuniasse, P. *J. Am. Chem. Soc.* **2006**, *128*, 16190–16205.
(29) Schalon, C.; Surgand, J.-S.; Kellenberger, E.; Rognan, D. *Proteins* **2008**, *71*, 1755–1778.
(30) Weil, N.; Rognan, D. *J. Chem. Inf. Model.* **2010**, *50*, 123–135.
(31) Barron, L. D. *Space Sci. Rev.* **2008**, *135*, 187–201.
(32) Lu, H. *Expert Opin. Drug Metab. Toxicol.* **2007**, *3*, 149–158.
(33) Klumpp, C.; Burger, A.; Mislin, G. L.; Abdallah, M. A. *Bioorg. Med. Chem. Lett.* **2005**, *15*, 1721–1724.
(34) Youard, Z. A.; Reimmann, C. *Microbiology* **2010**, *156*, 1772–1782.
(35) Froimowitz, M.; Rämsby, S. *J. Med. Chem.* **1991**, *34*, 1707–1714.
(36) Surgand, J. S.; Rodrigo, J.; Kellenberger, E.; Rognan, D. *Proteins* **2006**, *62*, 509–538.
(37) Joshi, D.; Völkl, M.; Shepherd, G. M.; Laska, M. *Chem. Senses* **2006**, *31*, 655–664.
(38) Sambrook, J.; Russell, D. W. *Molecular Cloning: A Laboratory Manual*; Cold Spring Harbor Lab Press: Cold Spring Harbor, NY, 2001.
(39) Schnider, U.; Keel, C.; Blumer, C.; Troxler, J.; Défago, G.; Haas, D. *J. Bacteriol.* **1995**, *177*, 5387–5392.
(40) Laville, J.; Blumer, C.; Von Schroetter, C.; Gaia, V.; Defago, G.; Keel, C.; Haas, D. *J. Bacteriol.* **1998**, *180*, 3187–3196.
(41) Stanisich, V. A.; Holloway, B. W. *Genet. Res.* **1972**, *19*, 91–108.
(42) Hoegy, F.; Celia, H.; Mislin, G. L.; Vincent, M.; Gallay, J.; Schalk, I. J. *J. Biol. Chem.* **2005**, *280*, 20222–20230.
(43) Cobessi, D.; Meksem, A.; Brillet, K. *Proteins* **2010**, *78*, 286–294.
(44) Roth, M.; Carpentier, P.; Kaikati, O.; Joly, J.; Charrault, P.; Pirocchi, M.; Kahn, R.; Fanchon, E.; Jacquamet, L.; Borel, F.; Bertoni, A.; Israel-Gouy, P.; Ferrer, J. L. *Acta Crystallogr., Sect. D* **2002**, *58*, 805–814.
(45) Kabsch, W. *J. Appl. Crystallogr.* **1993**, *26*, 795–800.
(46) McCoy, A. J.; Grosse-Kunstleve, R. W.; Adams, P. D.; Winn, M. D.; Storoni, L. C.; Read, R. J. *J. Appl. Crystallogr.* **2007**, *40*, 658–674.
(47) Collaborative Computational Project, Number 4. *Acta Crystallogr., Sect. D* **1994**, *50*, 760−763.
(48) Emsley, P.; Cowtan, K. *Acta Crystallogr., Sect. D* **2004**, *60*, 2126–2132.
(49) Adams, P. D.; Grosse-Kunstleve, R. W.; Hung, L. W.; Loerger, T. R.; McCoy, A. J.; Moriarty, N. W.; Read, R. J.; Sacchettini, J. C.; Sauter, N. K.; Terwilliger, T. C. *Acta Crystallogr., Sect. D* **2002**, *58*, 1948–1954.
(50) Murshudov, G. N.; Vagin, A. A.; Dodson, E. J. *Acta Crystallogr., Sect. D* **1997**, *53*, 240–255.
(51) Brunger, A. T. *Nature* **1992**, *355*, 472–475.
(52) Laskowski, R. A.; Macarthur, M. W.; Moss, D. S.; Thornton, J. M. *J. Appl. Crystallogr.* **1993**, *26*, 283–291.
(53) Hooft, R. W.; Vriend, G.; Sander, C.; Abola, E. E. *Nature* **1996**, *381*, 272.
(54) Chen, V. B.; Arendall, W. B.; Headd, J. J.; Keedy, D. A.; Immormino, R. M.; Kapral, G. J.; Murray, L. W.; Richardson, J. S.; Richardson, D. C. *Acta Crystallogr., Sect. D* **2010**, *66*, 12–21.
(55) Delano, W. L. *The PyMOL Molecular Graphics System*; DeLano Scientific: Palo Alto, CA, 2002.
(56) *SymyxDraw*; Accelrys Inc.: San Diego, CA, 2011.
(57) Sadowski, J.; Schwab, C. H. *Computational Medicinal Chemistry and Drug Discovery*; Bultinck, P., De Winter, H., Langenaeker, W., Tollenaere, J. P., Eds.; Dekker Inc.: New York, 2004; pp 151−212.
(58) Verdonk, M. L.; Cole, J. C.; Hartshorn, M. J.; Murray, C. W.; Taylor, R. D. *Proteins* **2003**, *52*, 609–623.
(59) *SYBYL-X 1.2*; Tripos International: St. Louis, MO, 2011.
(60) Marcou, G.; Rognan, D. *J. Chem. Inf. Model.* **2007**, *47*, 195–207.